Journal of Materials Chemistry

Cite this: DOI: 10.1039/c0jm03405c

www.rsc.org/materials

PAPER

Role of photoactive layer morphology in high fill factor all-polymer bulk heterojunction solar cells†

S. Fabiano,[ac] Z. Chen,[b] S. Vahedi,[b] A. Facchetti,[b] B. Pignataro[c] and M. A. Loi*[a]

Received 9th October 2010, Accepted 6th January 2011
DOI: 10.1039/c0jm03405c

We report on the realization of all-polymer solar cells based on blends of poly(3-hexylthiophene-2,5-diyl) (P3HT) as a donor and poly{[*N*,*N*′-bis(2-octyldodecyl)-naphthalene-1,4,5,8-bis(dicarboximide)-2,6-diyl]-*alt*-5,5′-(2,2′-bithiophene)} (P(NDI2OD-T2)) as an acceptor. High fill factors are demonstrated for the first time in this class of devices suggesting high dissociation efficiency for the bounded electron–hole pairs and balanced electron and hole mobility along the thin films. The use of the high-mobility n-type P(NDI2OD-T2) polymer enables us to overcome one of the problems limiting the efficiency of all-polymer solar cells, resulting in fill factors comparable with those reported for fullerene-based devices.

Introduction

Solution-processed polymer solar cells (PSCs) have attracted great interest during the last few years as a promising low-cost alternative to the conventional silicon-based photovoltaic devices.[1,2] The fabrication of these devices by solution-processing the photoactive layer offers an important advantage to enable flexible, roll-to-roll and large-area photovoltaic technologies.[3] A breakthrough in this field originated in the engineering of ordered thin film bulk heterojunction (BHJ) solar cells composed of electron donor (D) and electron acceptor (A) semiconductors as the photoactive layer.[4,5] To date, the most efficient PSCs are based on polymer/fullerene derivative blends[6] and the design/synthesis of new p-type polymers has dramatically improved the power conversion efficiencies (PCEs), now surpassing 7%.[7] However, due to the low extinction coefficient of the fullerene derivatives, only a limited part of the solar spectrum is generally harvested.[8] In this respect, polymer (donor)/polymer (acceptor) blends may offer several advantages compared to the polymer/fullerene ones. By tuning the absorption profile of each component, all-polymer blends may allow for covering complementary parts of the solar spectrum thus improving the final power conversion efficiency.[9,10] On the other hand, blending of two polymers generally results into microscopic phase separation which dramatically reduces the donor–acceptor interfacial area thus reducing exciton dissociation probability. Such donor and/or acceptor morphological domains must be reduced to the size of the exciton diffusion length (*ca.* 5–10 nm), in order to enhance the PCE.[11–13]

Promising results have been reported so far for all-polymer solar cells and efficiencies approaching 2% have been demonstrated.[13–16] Unfortunately, such performances are relatively poor as compared to those of fullerene-based devices. One of the main reasons limiting the efficiency of the all-polymer SCs is the low fill factor (FF), typically less than 30%. Although the origin of the reduced FF in all-polymer SCs has not been fully clarified, it is largely attributed to a low dissociation efficiency of the bound electron–hole pairs. The low dielectric constant of polymer with respect to the fullerenes, the unfavorable mixing properties of the macromolecules, as well as the low bulk carrier mobility are some of the loss mechanisms contributing to limit the FF. The employment of low-performing n-type polymers, for example, results in unbalanced bulk carrier transports where the electron mobility is far lower than the hole mobility, leading to space-charge effects.[17] Kim *et al.* have shown that the low electron mobility of poly(9,9-dioctylfluorene-*co*-benzothiadiazole) (F8BT) is mainly responsible for the reduced FF (*ca.* 36%) of the all-polymer SCs of this polymer in the blend with regioregular poly(3-hexylthiophene-2,5-diyl) (P3HT), demonstrating the PCE of 0.13%.[18] Thus, new high-mobility n-type polymers are needed to improve the efficiency of all-polymer SCs.

Herein, we report the realization of all-polymer solar cells based on the blend of poly{[*N*,*N*′-bis(2-octyldodecyl)-naphthalene-1,4,5,8-bis(dicarboximide)-2,6-diyl]-*alt*-5,5′-(2,2′-bithiophene)} (P(NDI2OD-T2), ActivInk™ N2200)[19] as an electron acceptor and P3HT as an electron donor. The use of P(NDI2OD-T2) enables us to reach high fill factor close to 70%, indicating a large balanced electron and hole mobility. A solvent

[a]*Zernike Institute for Advanced Materials, University of Groningen, Nijenborgh 4, 9747 AG Groningen, The Netherlands. E-mail: m.a.loi@rug.nl*
[b]*Polyera Corporation, 8045 Lamon Avenue, Skokie, IL, 60077, USA*
[c]*Dipartimento di Chimica "S. Cannizzaro", Università degli studi di Palermo, V.le delle Scienze-Parco D'Orleans II, ed. 17-90128 Palermo, Italy*

† Electronic supplementary information (ESI) available: Additional AFM images and *J*–*V* characteristics for devices with Sm contacts. See DOI: 10.1039/c0jm03405c

dependence of the PCE was observed, suggesting that the optimization of the final active layer morphology could be one of the factors limiting the efficiency.

Experimental section

Materials and device fabrication

The poly{[*N*,*N*′-bis(2-octyldodecyl)-naphthalene-1,4,5,8-bis(dicarboximide)-2,6-diyl]-*alt*-5,5′-(2,2′-bithiophene)} (P(NDI2OD-T2), ActivInk™ N2200) was obtained from Polyera Corporation, USA. A batch with a molecular weight of ~250 kDa and a PDI of ~5 was used. The P(NDI2OD-T2) was blended with regioregular poly(3-hexylthiophene-2,5-diyl) (P3HT) purchased from Rieke Metals with regioregularity >98% and average molecular weight <50 kDa.

The photovoltaic property of the blend was studied in the device structure composed of ITO/PEDOT:PSS/polymer blend/LiF/Al. Indium tin oxide (ITO)-coated glass substrates were cleaned stepwise in soap, demineralized water, acetone and isopropanol under ultrasonication for 5 min each and subsequently dried in an oven at 140 °C for 10 min. The substrates were then treated with ultraviolet ozone plasma for 20 min. A thin layer (~50 nm) of PEDOT:PSS (Clevios P VP AI 4083) was spin-coated onto the cleaned ITO substrates and annealed in an oven at 140 °C for 10 min. The substrates were transferred into a nitrogen-filled glovebox (<0.1 ppm O_2 and H_2O) for the active layer coating and electrode deposition. The polymer blends, having different donor–acceptor weight ratios, were spin-coated on the PEDOT:PSS-coated substrates with an active layer thickness of 80–110 nm from chlorobenzene (CB), *o*-dichlorobenzene (*o*-DCB) and xylene (Xy) solutions after filtration with a 0.45 μm PTFE syringe filter. Variations of few tens of nanometres in the active layer thickness were not observed influencing significantly the device performance. The film thickness was measured by using a DekTak II profilometer. Metal contacts were fabricated by thermal evaporation at a pressure <10^{-6} mbar with a device area of 4 mm^2, as defined by a shadow mask.

Characterization methods

Current–voltage characteristics were measured inside the glovebox by using a Keithley 2400 source/measure unit under AM 1.5 G illumination at 100 mW cm^{-2}. The incident-photon-to-converted-current efficiency (IPCE) was measured using a lock-in amplifier (SR830, Stanford Research Systems) coupled with a monochromator and a xenon lamp under short-circuit condition.

Absorption measurements were performed on freshly prepared thin films by using a Perkin Elmer Lambda 900 spectrometer.

The morphology of the active layers has been inspected by atomic force microscopy (AFM) in air using a Multimode Nanoscope IV (Digital Instruments, Santa Barbara, CA) working in a tapping mode. Etched-silicon probes with a pyramidal-shape tip having a nominal curvature of 10 nm and a nominal internal angle of 35° were used. The height and phase-lag images were obtained by raster scanning 512 × 512 points with a scan rate below 1 line per second at a tip resonance frequency of 330 kHz.

Results and discussion

The chemical structures of regioregular P3HT and P(NDI2OD-T2), along with the relative energy level diagram and absorption spectra are shown in Fig. 1. The HOMO and LUMO level offsets of the two polymers are optimal for an efficient charge transfer, as was recently demonstrated by time-resolved photoluminescence measurements.[20] The LUMO levels of P3HT and P(NDI2OD-T2) are ~3.2 and 4.0 eV, respectively. A theoretical open circuit voltage (V_{oc}) of about 0.9 V is expected, as generally expressed by the energy difference between the HOMO of the donor and the LUMO of the acceptor minus a loss of 0.3 eV.[21,22] In addition, the narrow band gap of both polymers (*ca.* 1.7 eV for P3HT and *ca.* 1.6 eV for P(NDI2OD-T2)) allows to extend the light absorption of the blend up to 850 nm, covering complementary regions of the visible range (see Fig. 1b). The absorption spectrum of the P3HT/P(NDI2OD-T2) blend is simply the superposition of the two polymers absorption spectra, indicating that no charge transfer occurs at the ground state.

To test the photovoltaic properties of the polymer-blend thin films, all devices were fabricated on PEDOT:PSS-coated indium tin oxide substrates. Fig. 2 shows the *J*–*V* characteristics of the P3HT/P(NDI2OD-T2) solar cells with 1 : 1 and 1 : 2 weight ratio (w/w) both from CB and *o*-DCB. An enhancement of the device photovoltaic performances is observed when the P(NDI2OD-T2) concentration in the polymer-blend is increased. However, no

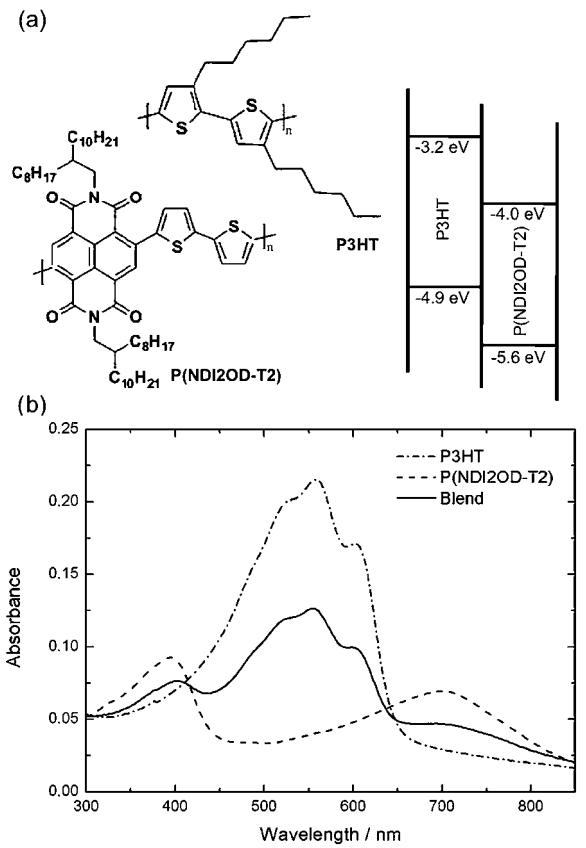

Fig. 1 (a) Chemical structures and energy level diagram of P(NDI2OD-T2) and P3HT. (b) Absorption spectra of P3HT (dash-dotted line), P(NDI2OD-T2) (dashed line) and blend (solid line) thin films.

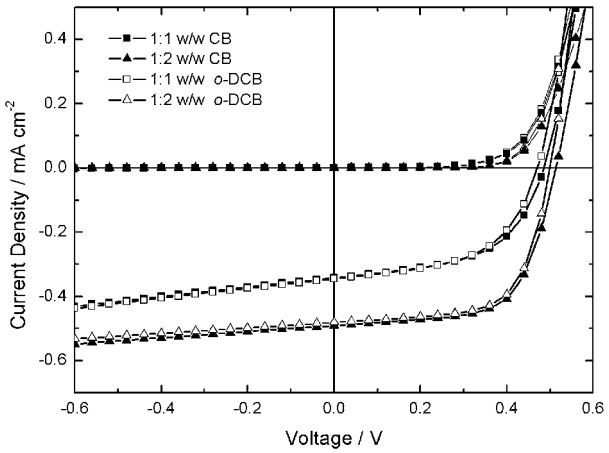

Fig. 2 Current density–voltage (J–V) characteristics for 1 : 1 and 1 : 2 w/w P3HT/P(NDI2OD-T2) solar cells spin-coated from CB and *o*-DCB.

significant improvements were observed when the P(NDI2OD-T2) content in the blend was increased further. The effect of the D/A weight ratio along with the influence of the solvent on the photovoltaic behaviour of the PSC is summarized in Table 1. The observed open circuit voltage is consistent with the $HOMO_D$ - $LUMO_A$ difference expected from the energy level of P3HT and P(NDI2OD-T2). Indeed, according to the typical energy loss in P3HT-based cells (*ca.* 0.35 V),[23] the maximum predictable open circuit voltage for our devices should be ~0.55 V, which is in agreement with the experimental results.

Interestingly, the fill factor values of these devices are the highest reported so far for all-polymer solar cells, suggesting a high charge separation efficiency and the balanced carrier mobility for P3HT/P(NDI2OD-T2) blends. In this respect, the P3HT/P(NDI2OD-T2) interface has been shown to be highly efficient for charge transfer[20] and free carrier generation.[24] Furthermore, a recent study shows that P(NDI2OD-T2) films exhibit a large bulk electron mobility in a diode architecture ($\sim 5 \times 10^{-3}$ cm^2 V^{-1} s^{-1}),[25] which is comparable to the typical bulk hole mobility of P3HT films ($\sim 2 \times 10^{-3}$ cm^2 V^{-1} s^{-1}).[18] We also showed that P3HT/P(NDI2OD-T2) blends yield high balanced ambipolar mobilities ($\sim 3 \times 10^{-3}$ cm^2 V^{-1} s^{-1}) in FET configuration.[20] Despite these favourable charge transport conditions, our devices exhibit modest short-circuit current densities (J_{sc} = 0.34 ÷ 0.49 mA cm^{-2}), resulting in low power conversion efficiencies (PCE = 0.09 ÷ 0.16%).

Contact-limited currents have been observed for P(NDI2OD-T2), even when low work function metals are employed.[25] We performed J–V measurements on devices with samarium (Sm) contacts, which has been reported[25] being the best injecting electrode for this n-type polymer. No significant differences in the extracted currents were observed when Sm was employed, with FF values comparable to those achieved with LiF/Al (see Fig. S1 in the ESI†).

To evaluate if the recombination processes are limiting the device performance, light intensity dependent measurements were carried out on the most efficient devices. Since no significant photovoltaic performance differences are observed for devices spin-coated from CB and *o*-DCB, this study was carried out on 1 : 2 w/w P3HT/P(NDI2OD-T2) cells spin-coated from CB. The relationship between J_{sc} and the light intensity is expressed as $J_{sc} \propto I^{\alpha}$, with α generally ranging from 0.85 to 1.[26] As shown in Fig. 3, a linear dependence of the short-circuit current density on the light intensity (law fit to $\alpha = 1.01$) was observed. These data suggest that major charge carrier losses are due to monomolecular (exciton or geminate pair) recombination processes and not due to bimolecular recombination, since in the latter case a sub-linear dependence of the J_{sc} is expected.[27] Furthermore, as observed for Langevin recombination in polymer/fullerene devices, the open circuit voltage depends on the light intensity with a kT/q slope.[28] Stronger dependence has been observed for the all-polymer solar cells and explained by electron trap-assisted recombination mechanisms.[29] In our case, a dependence with a slope of $1.3kT/q$ was observed (Fig. 3). A similar dependence of the open circuit voltage has been reported for a graded bilayer structure of M3EH-PPV (donor polymer) and CN-ether-PPV (acceptor polymer) solar cells, for which a vertical composition gradient with the CN-ether-PPV rich phase on the top of the polymer-blend films has been proposed.[15]

To evaluate the role of the blend morphology, the topography of the thin films was investigated by atomic force microscopy (AFM). The tendency of the polymer–polymer blends to phase-separate is generally ascribed to a low entropy of mixing and is governed by a spinodal decomposition of the blend.[30] Fig. 4 refers to 1 : 2 w/w P3HT/P(NDI2OD-T2) polymer-blend films spin-coated from CB (a and c) and *o*-DCB (b and d). In particular, a fiber-like structure of the surfaces is visible both in topography (a and b) and in phase-lag (c and d) images. The

Table 1 Summary of device performance parameters for the ITO/PEDOT:PSS/P3HT:P(NDI2OD-T2)/LiF/Al solar cells shown in Fig. 2

	J_{sc}/mA cm^{-2}	V_{oc}/V	FF (%)	PCE (%)
1 : 1 CB	0.34	0.49	54	0.09
1 : 2 CB	0.49	0.51	66	0.16
1 : 1 *o*-DCB	0.35	0.48	54	0.09
1 : 2 *o*-DCB	0.48	0.50	67	0.16

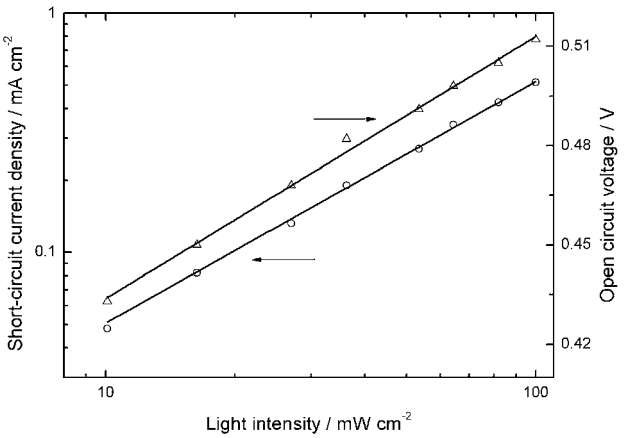

Fig. 3 Light intensity dependence of the short-circuit current density (open circle) and the open circuit voltage (open triangle) for a 1 : 2 w/w P3HT/P(NDI2OD-T2) solar cell from CB. The relationship between J_{sc} and the light intensity is expressed as $J_{sc} \propto I^{\alpha}$.

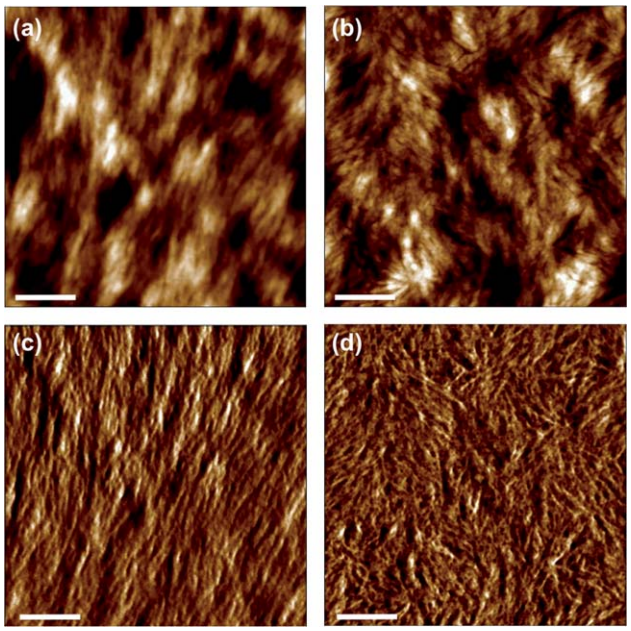

Fig. 4 AFM topography (a and b) and phase-lag (c and d) images of 1 : 2 w/w P3HT/P(NDI2OD-T2) thin films from CB (a and c) and *o*-DCB (b and d). All scale bars are 200 nm.

RMS roughness at 1 × 1 μm is equal to 1.73 nm for the thin films from CB and 1.65 nm for those from *o*-DCB with a feature size of the order of 10–35 nm (see Fig. S2 in the ESI†). Such a morphology has been already observed for the pristine P(NDI2OD-T2)[19] and justified by a face-on molecular packing with a high in-plane order.[31] Such a morphological similarity between the blend and the pristine polymer surface could suggest a vertical phase segregation of the polymer–polymer blend.

Vertically phase-separated structures have been observed for several spin-coated polymer blends upon evaporation of the solvent.[15,18] Since the typical exciton diffusion length in the organic semiconductors is of the order of *ca.* 5–7 nm,[32] in a bilayer-like structure only a narrow layer near to the planar heterojunction is involved in the photovoltaic process, strongly limiting the device performance.[33] Recently, inverted bilayer solar cells of P3HT and P(NDI2OD-T2) have been realized by soft-contact lamination of the two polymers, showing FF > 55% but only very moderate J_{sc} (0.069 ÷ 0.082 mA cm^{-2}).[34] Moreover, the balanced electron and hole mobility described above for our field-effect transistor measurements on P3HT/P(NDI2OD-T2) blends may be justified by the formation of horizontally phase separated pathways for both polymers between the transistor electrodes.[20,35] Considering the morphological features observed for the D/A films along with the other experimental evidence, we proposed a vertical phase separation with a P(NDI2OD-T2) rich phase on the top of the photoactive films.

Accordingly, in order to improve the lateral phase separation of the P3HT/P(NDI2OD-T2) blend, xylene was used as a solvent. It is well-known that the P3HT self-organizes in crystalline aggregates with the enhanced hole mobility when spin-coated from poor solvents such as xylene.[36] In this solvent, the self-assembly of the P3HT occurs readily in the solution, leading to whisker-like nanostructures that increase the bulk D/A interface along the thin films with the formation of percolation pathways useful for the charge transport.[37,38] An improvement, for example, in the short-circuit current by a factor of 10 has been observed when P3HT nanofibers are incorporated into the blend with polyfluorene copolymers (*i.e.* F8BT), as compared to the as-cast blends without fibers.[37] The AFM topography (a and c) along with the phase-lag (b and d) images relative to the 1 : 1 (a and b) and the 1 : 2 (c and d) w/w P3HT/P(NDI2OD-T2) polymer-blend films is shown in Fig. 5. Laterally phase-separated nanostructures are visible in both topography and phase-lag images. In particular, the 1 : 1 w/w ratio shows domains of the order of 180–230 nm as well as a finer phase separation (less than 20 nm). Fibers as wide as 50–90 nm are evident for the 1 : 2 w/w blend (see Fig. S3 in the ESI†). The RMS roughness at 1 × 1 μm is about 2.80 and 2.11 nm for the 1 : 1 and 1 : 2 w/w P3HT/P(NDI2OD-T2), respectively.

The resulting *J*–*V* characteristic of the xylene-processed solar cell is shown in Fig. 6. A short-circuit current density of 1.02 mA cm^{-2} was observed for the 1 : 1 w/w devices. The J_{sc} is at least 2–3× higher than the best results obtained from CB and *o*-DCB for the same weight ratio (*ca.* 0.35 mA cm^{-2}). This result is consistent with a more efficient lateral phase separation with respect to a self-stratified one as shown by the AFM analysis. Moreover, the current density increases to 2.39 mA cm^{-2} for the devices with D/A weight ratio of 1 : 2. However, a reduction in the current was observed with a further increase in the P(NDI2OD-T2) content. The V_{oc} values did not differ from those observed for CB and *o*-DCB, and were 0.49 V and 0.48 V for 1 : 1 and 1 : 2 w/w, respectively. The FF decreases from 60 to 54% with the increase in the acceptor content in the blend. Although these FF values are very high when compared to those of other all-polymer SCs, the lowest values are consistent with an increased internal resistance derived from the formation of isolated laterally phase-separated domains.[39] The resulting PCE

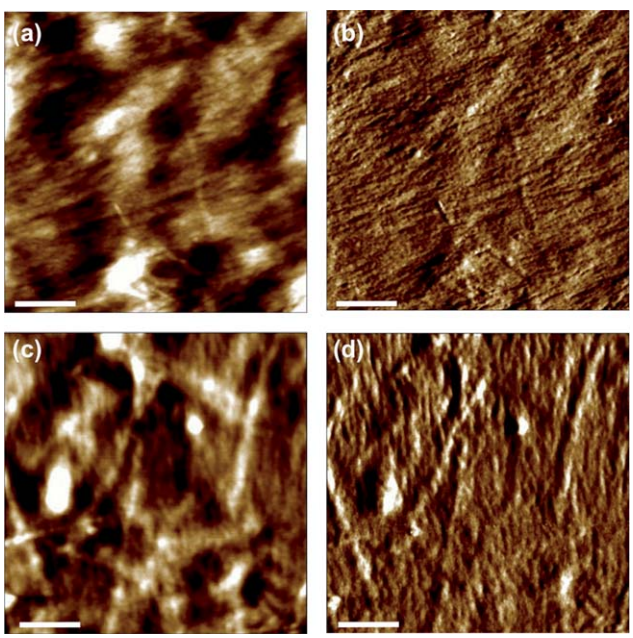

Fig. 5 AFM topography (a and c) and phase-lag (b and d) images of 1 : 1 (a and b) and 1 : 2 (c and d) w/w P3HT/P(NDI2OD-T2) thin films spin-coated from xylene. All scale bars are 200 nm.

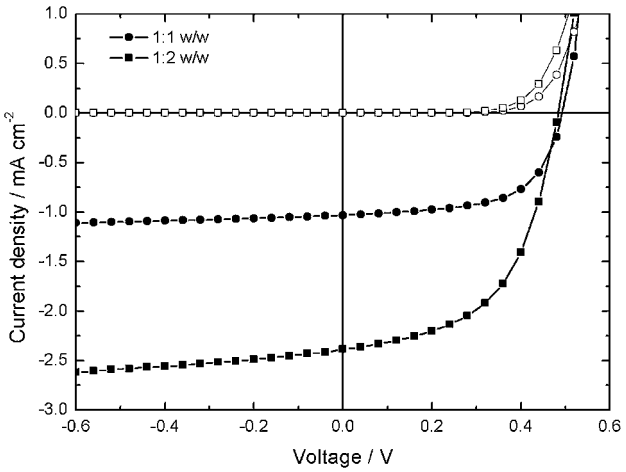

Fig. 6 *J–V* characteristics for 1 : 1 and 1 : 2 w/w P3HT/P(NDI2OD-T2) solar cells from xylene.

increases from 0.28% for the 1 : 1 w/w to 0.62% for the 1 : 2 w/w D/A blends.

Fig. 7 shows the incident-photon-to-converted-electron efficiency (IPCE) relative to the devices reported in Fig. 6. The maximum IPCE was found to be *ca.* 8.5% and 15.8% at 520 nm for 1 : 1 and 1 : 2 w/w cells, respectively. This wavelength is close to the maximum absorption of P3HT (~550 nm). In addition, a shoulder at *ca.* 600 nm is visible in both the IPCE spectra, related to the self-assembly of the P3HT polymer chains.[40] For wavelengths longer than 650 nm, the IPCE spectra are dominated by the absorption of P(NDI2OD-T2) having a maximum at *ca.* 700 nm and indicating that a non-negligible portion of the excitons is generated in the acceptor domains. The IPCE analysis shows that it is possible therefore to extend the photon absorption and the relative electron conversion up to 850 nm, by using P(NDI2OD-T2) as the acceptor.

It should be noted that the optimal blend ratio is different from that commonly used in polymer–fullerene systems.[41] The dependence of the photovoltaic performance on the weight ratio of P3HT/P(NDI2OD-T2) could be explained in terms of

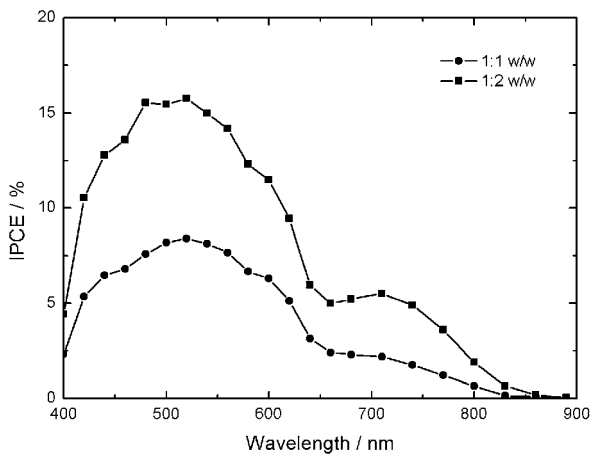

Fig. 7 *J–V* characteristics for 1 : 1 and 1 : 2 w/w P3HT/P(NDI2OD-T2) solar cells from xylene.

absorption and phase separation in the polymer-blend films. The increase in J_{sc} and PCE with the P(NDI2OD-T2) content in the blend indeed can be mainly ascribed to the extended photon absorption. Further increasing the P(NDI2OD-T2) concentration may lead to large demixing in the polymer blend, which negatively affects the electron transport.

Conclusion

We have studied the photovoltaic properties of the P(NDI2OD-T2) in the blend with the P3HT. High fill factor in all-polymer solar cells have been demonstrated for the first time with values of nearly 70%, suggesting a highly balanced mobility into the polymer-blend thin films. Thus, using high mobility electron-transporting polymers such as P(NDI2OD-T2) enables FF values comparable with those reported for fullerene-based devices. However, several limiting factors still hinder to reach high efficiencies as for instance the photoactive blend morphology, thus further optimizations are necessary. The use of additive molecules may eventually lead to a better morphology and to an overall improvement of the device performance. In addition, the electronic structure of the blend could play an important role on the ultimate efficiency. Adjusting the D and A HOMO and LUMO levels by combining P(NDI2OD-T2) with new high-performing p-type polymers would allow us to minimize the energy loss due to the LUMO offset.

Acknowledgements

We thank F. van der Horst and J. Harkema for technical assistance.

References

1 N. S. Lewis, *Science*, 2007, **315**, 798–801.
2 A. C. Mayer, S. R. Scully, B. E. Hardin, M. W. Rowell and M. D. McGehee, *Mater. Today*, 2007, **10**, 28–33.
3 F. C. Krebs, *Sol. Energy Mater. Sol. Cells*, 2009, **93**, 394–412.
4 J. J. M. Halls, C. A. Walsh, N. C. Greenham, E. A. Marseglia, R. H. Friend, S. C. Moratti and A. B. Holmes, *Nature*, 1995, **376**, 498–500.
5 G. Yu, J. Gao, J. C. Hummelen, F. Wudl and A. J. Heeger, *Science*, 1995, **270**, 1789–1791.
6 B. C. Thompson and J. M. J. Fréchet, *Angew. Chem., Int. Ed.*, 2008, **47**, 58–77.
7 H.-Y. Chen, J. Hou, S. Zhang, Y. Liang, G. Yang, Y. Yang, L. Yu, Y. Wu and G. Li, *Nat. Photonics*, 2009, **3**, 649–653.
8 T. J. Savenije, J. E. Kroeze, X. Yang and J. Loos, *Adv. Funct. Mater.*, 2005, **15**, 1260–1266.
9 G. Sang, E. Zhou, Y. Huang, Y. Zou, G. Zhao and Y. Li, *J. Phys. Chem. C*, 2009, **113**, 5879–5885.
10 G. Sang, Y. Zou, Y. Huang, G. Zhao, Y. Yang and Y. Li, *Appl. Phys. Lett.*, 2009, **94**, 193302.
11 C. R. McNeill, S. Westenhoff, C. Groves, R. H. Friend and N. C. Greenham, *J. Phys. Chem. C*, 2007, **111**, 19153–19160.
12 S. Fabiano and B. Pignataro, *Phys. Chem. Chem. Phys.*, 2010, **12**, 14848–14860.
13 S. Cataldo, S. Fabiano, F. Ferrante, F. Previti, S. Patanè and B. Pignataro, *Macromol. Rapid Commun.*, 2010, **31**, 1281–1286.
14 C. R. McNeill, A. Abrusci, J. Zaumseil, R. Wilson, M. J. McKiernan, J. H. Burroughes, J. J. M. Halls, N. C. Greenham and R. H. Friend, *Appl. Phys. Lett.*, 2007, **90**, 193506.
15 T. Kietzke, H.-H. Hörhold and D. Neher, *Chem. Mater.*, 2005, **17**, 6532–6537.
16 T. W. Holcombe, C. H. Woo, D. F. J. Kavulak, B. C. Thompson and J. M. J. Frèchet, *J. Am. Chem. Soc.*, 2009, **131**, 14160–14161.

17 V. D. Mihailetchi, J. Wildeman and P. W. M. Blom, *Phys. Rev. Lett.*, 2005, **94**, 126602.
18 Y. Kim, S. Cook, S. A. Choulis, J. Nelson, J. R. Durrant and D. D. C. Bradley, *Chem. Mater.*, 2004, **16**, 4812–4818.
19 H. Yan, Z. Chen, Y. Zheng, C. Newman, J. R. Quinn, F. Dötz, M. Kastler and A. Facchetti, *Nature*, 2009, **457**, 679–686.
20 K. Szendrei, D. Jarzab, Z. Chen, A. Facchetti and M. A. Loi, *J. Mater. Chem.*, 2010, **20**, 1317–1321.
21 C. J. Brabec, A. Cravino, D. Meissner, N. S. Sariciftci, T. Fromherz, M. T. Rispens, L. Sanchez and J. C. Hummelen, *Adv. Funct. Mater.*, 2001, **11**, 374–380.
22 D. Veldman, S. C. J. Meskers and R. A. J. Janssen, *Adv. Funct. Mater.*, 2009, **19**, 1939–1948.
23 A. Cravino, *Appl. Phys. Lett.*, 2007, **91**, 243502.
24 M. Rao, R. P. Ortiz, A. Facchetti, T. J. Marks and K. S. Narayan, *J. Phys. Chem. C*, 2010, **114**, 20609–20613.
25 R. Steyrleuthner, M. Schubert, F. Jaiser, J. C. Blakesley, Z. Chen, A. Facchetti and D. Neher, *Adv. Mater.*, 2010, **22**, 2799–2803.
26 L. J. A. Koster, V. D. Mihailetchi, H. Xie and P. W. M. Blom, *Appl. Phys. Lett.*, 2005, **87**, 203502.
27 J. Nelson, *Phys. Rev. B: Condens. Matter*, 2003, **67**, 155209.
28 L. J. A. Koster, V. D. Mihailetchi, R. Ramaker and P. W. M. Blom, *Appl. Phys. Lett.*, 2005, **86**, 123509.
29 M. M. Mandoc, W. Veurman, L. J. A. Koster, B. d. Boer and P. W. M. Blom, *Adv. Funct. Mater.*, 2007, **17**, 2167–2173.
30 R. A. L. Jones, *Phys. World*, 1995, **8**, 47.
31 J. Rivnay, M. F. Toney, Y. Zheng, I. V. Kauvar, Z. Chen, V. Wagner, A. Facchetti and A. Salleo, *Adv. Mater.*, 2010, **22**, 4359–4363.
32 O. V. Mikhnenko, F. Cordella, A. B. Sieval, J. C. Hummelen, P. W. M. Blom and M. A. Loi, *J. Phys. Chem. B*, 2008, **112**, 11601–11604.
33 C. J. Brabec, N. S. Sariciftci and J. C. Hummelen, *Adv. Funct. Mater.*, 2001, **11**, 15–26.
34 J. B. Kim, S. Lee, M. F. Toney, Z. Chen, A. Facchetti, Y. S. Kimand and Y.-L. Loo, *Chem. Mater.*, 2010, **22**, 4931–4938.
35 F. Dinelli, R. Capelli, M. A. Loi, M. Murgia, M. Muccini, A. Facchetti and T. J. Marks, *Adv. Mater.*, 2006, **18**, 1416–1420.
36 M. Mas-Torrent, D. d. Boer, M. Durkut, P. Hadley and A. P. H. J. Schenning, *Nanotechnology*, 2004, **15**, S265–S269.
37 T. Salim, S. Sun, L. H. Wong, L. Xi, Y. L. Foo and Y. M. Lam, *J. Phys. Chem. C*, 2010, **114**, 9459–9468.
38 S. Bertho, W. D. Oosterbaan, V. Vrindts, J. D'Haen, T. J. Cleij, L. Lutsen, J. Manca and D. Vanderzande, *Org. Electron.*, 2009, **10**, 1248–1251.
39 J. D. Servaites, S. Yeganeh, T. J. Marks and M. A. Ratner, *Adv. Funct. Mater.*, 2010, **20**, 97–104.
40 M. M. Erwin, J. McBride, A. V. Kadavanich and S. J. Rosenthal, *Thin Solid Films*, 2002, **409**, 198–205.
41 A. C. Mayer, M. F. Toney, S. R. Scully, J. Rivnay, C. J. Brabec, M. Scharber, M. Koppe, M. Heeney, I. McCulloch and M. D. McGehee, *Adv. Funct. Mater.*, 2009, **19**, 1173–1179.